A Novel Type-2 Fuzzy *C*-Means Clustering for Brain MR Image Segmentation

Pranaba K. Mishro, Sanjay Agrawal, *Member, IEEE*, Rutuparna Panda, *Member, IEEE*, and Ajith Abraham, *Senior Member, IEEE*

Abstract—The fuzzy *C*-means (FCM) clustering procedure is an unsupervised form of grouping the homogenous pixels of an image in the feature space into clusters. A brain magnetic resonance (MR) image is affected by noise and intensity inhomogeneity (IIH) during the acquisition process. FCM has been used in MR brain tissue segmentation. However, it does not consider the neighboring pixels for computing the membership values, thereby misclassifying the noisy pixels. The inaccurate cluster centers obtained in FCM do not address the problem of IIH. A fixed value of the fuzzifier (m) used in FCM brings uncertainty in controlling the fuzziness of the extracted clusters. To resolve these issues, we suggest a novel type-2 adaptive weighted spatial FCM (AWSFCM) clustering algorithm for MR brain tissue segmentation. The idea of type-2 FCM applied to the problem on hand is new and is reported in this article. The application of the proposed technique to the problem of MR brain tissue segmentation replaces the fixed fuzzifier value with a fuzzy linguistic fuzzifier value (M). The introduction of the spatial information in the membership function reduces the misclassification of noisy pixels. Furthermore, the incorporation of adaptive weights into the cluster center update function improves the accuracy of the final cluster centers, thereby reducing the effect of IIH. The suggested algorithm is evaluated using T1-w, T2-w, and proton density (PD) brain MR image slices. The performance is justified in terms of qualitative and quantitative measures followed by statistical analysis. The outcomes demonstrate the superiority and robustness of the algorithm in comparison to the state-of-the-art methods. This article is useful for the cybernetics application.

Index Terms—Adaptive weighted spatial FCM (AWSFCM), brain tissue segmentation, fuzzy *C*-means (FCM), MRI.

I. INTRODUCTION

THE ARTIFACTS in the neurological structure of the brain are the main challenging factor in the process of brain tissue segmentation. It is a procedure for obtaining the vital brain tissues, such as gray matter (GM), white matter (WM), and cerebrospinal fluid (CSF). Magnetic resonance (MR) imaging provides accurate information, such as 3-D information, high signal-to-noise ratio, excellent discrimination of soft tissues, and scientific information about the human brain anatomical structure for disease diagnosis. Therefore, it is the preferred modality for the diagnosis of the human brain.

However, it suffers from some considerable problems, such as noise and intensity inhomogeneity (IIH), out of which IIH is the most challenging obstacle. Numerous techniques are suggested to automate the brain tissue segmentation method, such as manual, intensity based, atlas based, and clustering [1]–[17].

Clustering is an unsupervised method that classifies the homogeneous data points in the feature space into clusters. Fuzzy *C*-means (FCM) clustering is considered as a standard soft clustering method for MR brain tissue segmentation. Several approaches are suggested to enhance the performance of the traditional FCM clustering procedure and to automate the tissue segmentation process. Ahmed *et al.* [18] suggested a modified FCM clustering procedure for estimation of the bias field. They proposed the segmentation of MRI data and intensity nonuniformity (INU) estimation using the modified fitness function of the standard FCM clustering algorithm. However, the method is restricted to single feature input. The authors suggested some more clinical evaluation and localized measurements. Their method is time consuming as the sum has to be computed for every pixel in each iteration.

Mohamed [19] suggested a modified FCM fitness function for segmentation of brain images. Their method follows the Markov random field (MRF) and filters the image while clustering for improving noise sensitivity. However, the noise performance is very limited as it does not incorporate the spatial information. The procedure is also limited in its application to a single-channel MRI scan or CT scan images only. Liew and Yan [20] presented an adaptive fuzzy clustering algorithm for 3-D MR image segmentation. Their process uses a dissimilarity index that accounts for the spatial continuity constraints for decreasing the effect of noise. However, the technique shows degraded performance for the segmentation of the CSF region.

It is to be noted that these methods do not include neighborhood information into the computation of the membership matrix and the cluster centers. The neighboring pixels convey approximately identical information of the content of an image. This spatial correlation of the neighboring pixels is essential in decreasing the impact of noise in a brain MR image.

Chuang *et al.* [21] suggested a spatial FCM clustering for image segmentation. They assimilated the neighborhood

information in the membership function. However, the algorithm is sensitive to a randomly defined membership matrix, which increases the computational complexity of the algorithm. Ji *et al.* [22] suggested a robust spatial-constrained FCM for the segmentation of brain MR images. The impact of the noisy pixels is overcome by constructing a spatial factor estimated from the posterior and prior probabilities and taking the spatial direction into consideration. This spatial factor plays the role of linear filters for smoothing the corrupted brain MR image. The IIH is taken care by combining the bias field model with the fuzzy fitness function. However, because of the nonconvex nature of the fitness function, the algorithm may be trapped in the local optima. Guo *et al.* [23] presented an adaptive FCM (AFCM) scheme using the noise detection for image segmentation. The technique uses two filtering methods for denoising and maintaining the details of the MR image. The parameters of the filters are computed using the variance of the intensity levels in each neighborhood. However, the authors used the standard FCM and did not indicate the effect of a constant fuzzifier value in determining accurate cluster centers.

Verma *et al.* [24] suggested an improved intuitionistic FCM (IIFCM) clustering technique using the advantage of intuitionistic fuzzy set theory. The intuitionistic fuzzy factor considering the similarity measure is incorporated in the membership function of the IIFCM procedure. This reduces the effect of noise and also estimates the boundaries of the tissue regions in the brain MR image. However, the authors have not considered the effect of a fixed fuzzifier value in finding accurate cluster centers. Adhikari *et al.* [25] suggested a conditional spatial FCM (csFCM) clustering technique. The algorithm incorporates an auxiliary variable into the membership function. This makes the technique more sensitive to the acquisition noise and the inhomogeneity in the tissue regions. Lei *et al.* [26] suggested the fast and robust FCM (FRFCM) by including the spatial information in its fitness function. This is to improve the computational efficiency and the robustness of the conventional FCM. Zhang *et al.* [27] suggested the deviation-sparse-based FCM with neighbor information (DSFCM_N) to estimate the spatial correlation in the neighborhood. However, the discussed approaches do not define any solution toward noise incurred due to the equidistant pixels and the uncertainty in the precise value of the parameters associated with fuzzy clustering. The dynamic range of input images for tissue segmentation has a high range of variation as it contains images from various modalities and various intensity of noise and IIH.

Assigning a fixed value to the fuzzifier (m) is not suitable for brain tissue segmentation. Hwang and Rhee [28] suggested the interval type-2 FCM (IT2FCM) clustering algorithm that derives the interval values of the fuzzifier (m_L, m_R) making the membership value more suitable. Here, the uncertainty of the fuzzifier is addressed but not resolved. Therefore, it is required to find suitable values of the fuzzifier called the linguistic fuzzifier (M). A general type-2 (GT2) approach to FCM clustering is a suitable model to define the uncertainty in the precise value of the fuzzifier [29]. As far as our knowledge is concerned, none of the techniques investigated the

type-2 FCM technique for brain tissue segmentation. This has inspired us to investigate the type-2 adaptive weighted spatial FCM (AWSFCM) clustering approach for the above problem. The GT2 FCM clustering procedure suggested by Linda and Manic [29] is a generalized technique to deal with various uncertain data points. The GT2 FCM clustering algorithm uses individual fuzzy sets with the secondary membership values.

In this article, we suggest a new scheme for MR brain tissue segmentation by using the type-2 FCM clustering algorithm with adaptive weights and spatial information. An optimized type-2 membership function is used to reduce the uncertainty in fuzzy clustering and the constraints. The membership values are calculated easily. An explicit formula for the partition membership matrix is introduced. The computation of the type-2 membership function using the fuzzy value of the linguistic fuzzifier (M) enhances the uncertainty modeling capability. The conversion from type-1 to type-2 clustering is clearly illustrated.

Usually, the spatial correlation is obtained by using an average filter approach prior to the clustering procedure. However, this approach is suitable for low noise and single feature input applications only. Therefore, we propose a Gaussian filter for the estimation of the spatial information. Krishnapuram and Keller [30] pointed out that if a data point is at an equal distance from multiple cluster centers, then its membership value will be equal for each cluster. These points are considered as the noise points and are assigned zero or a very low membership value. Our model includes an adaptive weight factor for the calculation of the new cluster centers and allocates larger weights to the pixels close to the expected decision boundary. We experimented with simulated brain MR images from the BrainWeb database [31] and real brain MR image from the Internet brain segmentation repository (IBSR) database [32]. The results obtained are compared with our implementations of the FCM [21], adaptive FCM (AFCM) [23], IIFCM [24], csFCM [25], FRFCM [26], DSFCM_N [27], IT2FCM [28], and GT2FCM [29] clustering procedures.

The remainder of this article is structured as follows. Section II explains the related works in fuzzy clustering. The suggested methodology is explained in Section III. The results and validations are discussed in Section IV. Finally, the concluding notes are provided in Section V.

II. RELATED WORK

The suggested method is compared with FCM, AFCM, IIFCM, csFCM, FRFCM, DSFCM_N, IT2FCM, and GT2FCM clustering algorithms. This section briefly explains the above-mentioned algorithms.

A. Type-1 Fuzzy C-Means

Fuzzy clustering is a practice to allocate a data point into a multiple number of clusters with a membership value. FCM is one of the standard fuzzy clustering procedures. For an image $X = \{x_1, x_2, \ldots, x_N\}$ with N number of pixels to be segmented into c number of clusters, the standard type-1 FCM

uses the following fitness function for clustering [17], [21]:

$$J_{\text{FCM}} = \sum_{j=1}^{N} \sum_{i=1}^{c} u_{ij}^m d_{ij}^2 \tag{1}$$

where u_{ij} is the membership value of a pixel x_j in the ith cluster with a cluster center y_i. The scalar exponent m known as the fuzzifier is any real number (> 1), $\| \cdot \|$ is the norm metric. The Euclidean distance $d_{ij} = (x_j - y_i)$ is computed between the pixel value and cluster centers. The membership values u_{ij} are calculated and updated as follows [21]:

$$u_{ij} = 1 \left/ \sum_{k=1}^{c} \left(\frac{d_{ij}}{d_{kj}}\right)^{2/(m-1)} \right. . \tag{2}$$

The membership values must satisfy the following criterion [21]:

$$\left\{ u_{ij} \in [0, 1] \right\} \left| \sum_{i=1}^{c} u_{ij} = 1 \quad \forall j \text{ and } 0 < \sum_{k=1}^{N} u_{ik} < N \forall i. \right. \tag{3}$$

Initially, the cluster centers are randomly selected and then updated with each iteration as follows [21]:

$$y_i = \sum_{j=1}^{N} u_{ij}^m x_j \left/ \sum_{j=1}^{N} u_{ij}^m \right. . \tag{4}$$

The algorithm is experimented with $m = 2$ and $c = 3$. This technique is successfully implemented for feature analysis, clustering, brain tissue segmentation, medical image processing, and target recognition.

B. AFCM

This approach is an improvement over the type-1 FCM. It incorporates neighboring gray-level variance in the fitness function represented by the following equation to denoise and maintain the resolution of the image. The fitness function of the model is developed using the probability of occurrence of local noise and is expressed as [23]

$$J_{\text{AFCM}} = \sum_{j=1}^{N} \sum_{i=1}^{c} u_{ij}^m \left\| \left[(1 - \gamma_j)\xi_j + \gamma_j \bar{x}_j\right] - y_i \right\| \tag{5}$$

where $\bar{x}_j$ is the mean of neighbors of the data point x_j. ξ_j is the weighted mean to compute the gray-level variance of the neighboring pixels. The probability γ_j of a pixel j being a noise point is computed as

$$\gamma_j = 1 - \left(\sum_{i \in N_j} \exp\left(\frac{-\|x_i - x_j\|^2}{\lambda_\gamma \max_{l \in N_j} \|x_l - x_j\|^2} \right) \middle/ N_R \right). \tag{6}$$

where λ_γ is a scaling parameter. N_j and N_R are the corresponding neighboring window and number of pixels in it.

The membership value and the cluster center are updated as

$$u_{ij} = \frac{\left\| \left[(1 - \gamma_j)\xi_j + \gamma_j \bar{x}_j\right] - y_i \right\|^{-2/(m-1)}}{\sum_{i=1}^{c} \left\| \left((1 - \gamma_j)\xi_j + \gamma_j \bar{x}_j\right) - y_i \right\|^{-2/(m-1)}} \tag{7}$$

$$y_i = \sum_{j=1}^{N} u_{ij}^m \left[(1 - \gamma_j)\xi_j + \gamma_j \bar{x}_j\right] \left/ \sum_{j=1}^{N} u_{ij}^m \right. . \tag{8}$$

The algorithm is tested with the parameters as $m = 2$ and $c = 3$, and the neighboring window size $w = 5 \times 5$.

C. IIFCM

This is a variant of the type-1 FCM to resolve the difficulties due to the ambiguous boundary between the tissue regions [24]. In this article, the local spatial information is incorporated using an intuitionistic fuzzy factor. The intuitionistic fuzzy factor H_{ij} is expressed as follows:

$$H_{ij} = \frac{1}{N_R} \sum_{j \in k} \frac{1}{d_{kj} + 1} \left[(1 - u_{ij})^m + (S_{ij})^m\right]$$
$$\text{for } 1 \le i \le c, 1 \le j \le N \tag{9}$$

where N_R is the number of neighboring pixels, u_{ij} is the membership value, and S_{ij} is the spatial membership value. The term d_{kj} is the Euclidian distance between the spatial coordinates as in [24]. The membership function is expressed as

$$u_{ij} = 1 \left/ \sum_{n=1}^{c} \left(\frac{d_{ij}^2 H_{ij}}{d_{nj}^2 H_{nj}}\right)^{1/(m-1)} \right. , 1 \le i \le c, 1 \le j \le N \tag{10}$$

where d_{ij} is the Euclidian distance between the pixel and the cluster centers. The centroid of the clusters can be computed using the following expression:

$$y_i = \min(\mu(y_i), v(y_i), \pi(y_i)) \tag{11}$$

where $\mu(y_i)$, $v(y_i)$, and $\pi(y_i)$ are the partial derivatives of the Lagrange function of the clusters. The algorithm is tested by using the parameters, $m = 2$ and $c = 3$, and the size of neighboring window $w = 3 \times 3$. The performance of the model is limited, as this algorithm does not incorporate the local spatial information into its membership value. It is to be noted that the fitness function of IIFCM is the same as that of FCM.

D. csFCM

This procedure incorporates an auxiliary conditional variable conforming to each data point [25]. It includes the local spatial information in the membership matrix. The spatial membership value is expressed as follows:

$$u_{ij} = f_{ij} \left/ \left(\|x_j - y_i\|^{2/(m-1)} \left/ \sum_{k=1}^{c} \|x_j - y_k\|^{2/(m-1)} \right. \right) \right. \tag{12}$$

where f_{ij} is the auxiliary conditional variable. It expresses the contribution of a data point x_j in the ith cluster and represented as $f_{ij} = \sum_{j \in N(x_j)} \mu_{ij}/N_R$. Here, μ_{ij} is the membership value of the data point x_j for the ith cluster and expressed as $\mu_{ij} = 1/(\|x_j - y_i\|^{2/(m-1)}/\sum_{k=1}^{c} \|x_j - y_k\|^{2/(m-1)})$. Note that N_R denotes the total number of pixels in the neighboring window. The spatial membership value is computed as follows:

$$Z_{ij} = (\mu_{ij})^p (u_{ij})^q \left/ \sum_{k=1}^{c} (\mu_{kj})^p (u_{kj})^q \right. \tag{13}$$

where p and q are the variables defining the relative significance of the membership values. The center of the cluster is determined as

$$y_i = \sum_{j=1}^{N} z_{ij}^m x_j \bigg/ \sum_{j=1}^{N} z_{ij}^m. \tag{14}$$

The spatial function incorporated in the membership matrix improves the robustness of the clustering procedure. The algorithm is experimented with the parameters, $m = 2, c = 3$, and $w = 3 \times 3$, and the controlling parameters $p = 2$ and $q = 2$. However, the performance is limited to a user-defined value of the fuzzifier (m).

E. FRFCM

In FRFCM [26], a faster membership filtering is introduced in place of the distance vector (between the pixel values and cluster centers). The objective function is minimized using the Lagrange function for the data point ($x_j = R^C(x)$) and its membership value (u_{ij}), where $R^C(x)$ is the morphological closing reconstruction of original image (x). The objective function is expressed as [26]

$$J_{FRFCM} = \sum_{j=1}^{N} \sum_{i=1}^{c} \gamma_j u_{ij}^m \|x_j - y_i\| - \lambda \left(\sum_{i=1}^{c} u_{ij} - 1 \right) \tag{15}$$

where $1 \leq j \leq N$, N is the number of pixels in the image. The Lagrange multiplier (λ) is used to find the saddle point of the Lagrange function. Here, γ_j is a relative constant, $\sum_{j=1}^{N} \gamma_j \leq N$. Furthermore, the membership values and cluster centers are updated as follows:

$$u_{ij} = \|x_j - y_i\|^{-2/(m-1)} \bigg/ \sum_{r=1}^{c} \|x_j - y_r\|^{-2/(m-1)} \tag{16}$$

$$y_i = \sum_{j=1}^{N} \gamma_j u_{ij}^m x_j \bigg/ \sum_{j=1}^{N} \gamma_j u_{ij}^m. \tag{17}$$

The technique uses local and spatial information for improving the segmentation results. Furthermore, the information preservation and denoising performance is improved by employing morphological operations. The technique is experimented by using the fuzzifier ($m = 2$), the cluster prototype value (c), and the size of neighboring window $w = 3 \times 3$.

F. DSFCM_N

The method introduced deviation and sparsity among the estimated value and actual values in a conventional FCM. By imposing the deviation and sparsity into FCM clustering, the objective function is expressed as [27]

$$J_{DSFCM\_N} = \sum_{i=1}^{c} \sum_{j=1}^{N} u_{ij}^m \left(\sum_{k \in N_j} \frac{1}{1 + d_{kj}} \|x_k - e_k - y_i\|_2^2 \right)$$
$$+ \sum_{t=1}^{l} \lambda_t \sum_{k \in N_j} \frac{\sum_{j=1}^{N} \|e_{jt}\|^p}{1 + d_{kj}} \tag{18}$$

where $p > 0$ and k is the neighbor of pixel j in the local window N_j. The Euclidean distance $d_{kj} = \|x_j - x_k\|$. e_k is the deviation vector of the neighbor pixels. $\lambda = (\lambda_1, \lambda_2, \ldots, \lambda_l)^T$ is a regulating vector of length l. The neighboring information is included as $\sum_{k \in N_j} \|x_k - e_k - y_i\|_2^2/(1 + d_{kj})$. Applying deviations, the membership values (u_{ij}) and cluster centers (y_i) are updated as follows:

$$u_{ij} = \left(\sum_{r=1}^{c} \left(\sum_{k \in N_j} \frac{1}{1 + d_{kj}} \|x_k - e_k - y_i\|^2 \bigg/ \right. \right.$$
$$\left. \left. \sum_{k \in N_j} \frac{1}{1 + d_{kj}} \|x_k - e_k - y_r\|^2 \right)^{1/m-1} \right)^{-1} \tag{19}$$

and

$$y_i = \left(\sum_{j=1}^{N} u_{ij}^m \sum_{k \in N_j} \frac{1}{1 + d_{kj}} (x_k - e_k) \right) \bigg/ \sum_{k \in N_j} \frac{1}{1 + d_{kj}} \sum_{j=1}^{N} u_{ij}^m. \tag{20}$$

The sparsity and deviation factors incorporated into the method improve the accuracy of cluster center estimation. This technique is tested on real MR images, by using the parameters, $m = 2, c = 3$, and $w = 3 \times 3$.

G. IT2FCM

In IT2FCM [28], the numeral value of the interval fuzzifier $[m_L, m_R]$ is computed in a possible linguistic interval rather than a specific value. Using the interval fuzzifier, the interval membership values are updated as

$$\underline{u}_i(x_j) = \min \left(1 \bigg/ \sum_{k=1}^{c} \left(\frac{\|x_j - y_i\|}{\|x_j - y_k\|} \right)^{\frac{2}{(m_L-1)}} \right.$$
$$\left. 1 \bigg/ \sum_{k=1}^{c} \left(\frac{\|x_j - y_i\|}{\|x_j - y_k\|} \right)^{\frac{2}{(m_R-1)}} \right) \tag{21}$$

$$\overline{u}_i(x_j) = \max \left(1 \bigg/ \sum_{k=1}^{c} \left(\frac{\|x_j - y_i\|}{\|x_j - y_k\|} \right)^{\frac{2}{(m_L-1)}} \right.$$
$$\left. 1 \bigg/ \sum_{k=1}^{c} \left(\frac{\|x_j - y_i\|}{\|x_j - y_k\|} \right)^{\frac{2}{(m_R-1)}} \right). \tag{22}$$

The cluster positions are updated as

$$[y_i^L, y_i^R] = \sum_{u(x_1) \in J_{x_1}} \cdots \sum_{u(x_1) \in J_{x_N}} \left(1 \bigg/ \frac{\sum_{j=1}^{N} x_j u_{ij}(x_j)^m}{\sum_{j=1}^{N} u_{ij}(x_j)^m} \right). \tag{23}$$

The position of each cluster can be obtained by defuzzifying the interval centroid values

$$y_i = (y_i^L + y_i^R)/2. \tag{24}$$

The algorithm is tested by using the interval fuzzifier in the range $m_L = 1.5$ and $m_R = 4$.

H. GT2FCM

This algorithm is designed to construct a secondary membership matrix $\tilde{U}$ using a fuzzy linguistic fuzzifier (M). This is to resolve the associated uncertainty in selection of the fuzzifier parameter (m) in FCM [29]. Using α-cut representation, the parameter M is expressed as

$$M = \bigcup_{\alpha \in [0,1]} \alpha / S_M(\alpha) \text{ where } S_M(\alpha) = \left[s_M^L(\alpha), s_M^R(\alpha) \right]. \quad (25)$$

Here, $\bigcup$ represents the union operation. The degree of belongingness of a pixel (x_j) in a cluster (y_i) is presented using the secondary membership matrix as

$$\left[\tilde{u}_i^L(x_j), \tilde{u}_i^R(x_j) \right] = \bigcup_{\alpha \in [0,1]} \alpha / \left[S_{\tilde{u}_i}^L(x_j|\alpha), S_{\tilde{u}_i}^R(x_j|\alpha) \right] \quad (26)$$

where $[S_{\tilde{u}_i}^L(x_j|\alpha), S_{\tilde{u}_i}^R(x_j|\alpha)]$ are the boundary conditions in the range of the interval linguistic fuzzifier $[s_M^L(\alpha), s_M^R(\alpha)]$.

The position of the centroids is obtained based on Liu's α-plane theorem as

$$C_{\tilde{u}_i} = \bigcup_{\alpha \in [0,1]} \alpha / \left[c_{\tilde{u}_i}^L(\alpha), c_{\tilde{u}_i}^R(\alpha) \right]. \quad (27)$$

The value of the cluster center (y_i) depends on the interval centroid $[c_{\tilde{u}_i}^L(\alpha), c_{\tilde{u}_i}^R(\alpha)]$ and computed as follows:

$$y_i = \sum_{i=1}^{K} z_i C_{\tilde{u}_i}(z_i) \Big/ \sum_{i=1}^{K} C_{\tilde{u}_i}(z_i) \quad (28)$$

where K is the discretization step number and z_i is the location vector of the discretized steps [29]. The algorithm is experimented with $c = 3$ and $K = 10$ for linguistic terms of fuzzifier.

III. PROPOSED METHODOLOGY

A. Type-2 AWSFCM Clustering

The suggested scheme is a novel extension of the GT2FCM clustering procedure. The uncertain value of the fuzzifier (m) has a significant influence in determining the position and the accuracy of the cluster partition (for high-range variation input data points). In this article, the difficulty due to the uncertain value of the fuzzifier is overcome using the linguistic terms as in the GT2FCM algorithm. The uncertainty in the input data points is converted to uncertain fuzzy partitions of the extracted clusters using the α-plane representation [33], [34]. Here, this approach is suggested for MR brain tissue segmentation. A schematic outline of the suggested technique is displayed in Fig. 1.

The algorithm is initiated using a user-defined interval fuzzifier range. These values are also called left and right fuzzifier values. The value of the linguistic fuzzifier (M) is determined in the given linguistic interval $[s_M^L(\alpha), s_M^R(\alpha)]$ using (25). This linguistic interval is used to determine the left and right type-1 membership values of the data points as

$$u_{ij}^L = 1 \Big/ \sum_{k=1}^{c} \left(\frac{\|x_j - y_i\|}{\|x_j - y_k\|} \right)^{\frac{2}{(s_M^L(\alpha)-1)}}$$
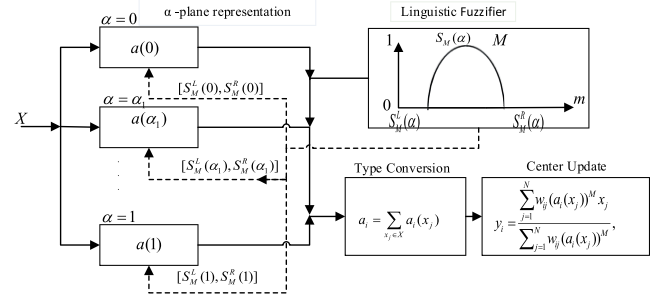

Fig. 1.   Schematic outline of the AWSFCM scheme.

$$u_{ij}^R = 1 \Big/ \sum_{k=1}^{c} \left(\frac{\|x_j - y_i\|}{\|x_j - y_k\|} \right)^{\frac{2}{(s_M^R(\alpha)-1)}}. \quad (29)$$

The spatial functions (h_{ij}^L, h_{ij}^R) are computed using the above membership values to represent the spatial information

$$h_{ij}^L = \sum_{k \in NB(x_j)} u_{ik}^L, \quad h_{ij}^R = \sum_{k \in NB(x_j)} u_{ik}^R \quad (30)$$

where the adaptive Gaussian filter is represented by the window centered on the pixel x_j. $NB(x_j)$ represents the neighbor membership of the pixel x_j, for incorporating the spatial information [21]. The Gaussian filter is adaptive in the sense that the order of the filter decreases with the convergence of the algorithm. In a similar way to the membership function, the spatial functions (h_{ij}^L, h_{ij}^R) represent the probability of pixel x_j in cluster y_i. This spatial function is included in the type-1 membership matrix to form new partition membership matrices ($u_{ij}^{'L}, u_{ij}^{'R}$) as

$$u_{ij}^{'L} = u_{ij}^{Lp} h_{ij}^{Lq} \Big/ \sum_{k=1}^{c} u_{kj}^{Lp} h_{kj}^{Lq}, \quad u_{ij}^{'R} = u_{ij}^{Rp} h_{ij}^{Rq} \Big/ \sum_{k=1}^{c} u_{kj}^{Rp} h_{kj}^{Rq}. \quad (31)$$

Here, p and q are the parameters to manage the relative significance of both the terms. The values of p and q are taken as 2 [25].

The partition membership matrices are used to express the type-2 membership matrices ($a_i^L(x_j), a_i^R(x_j)$). This is obtained using the given interval fuzzifier values $[s_M^L(\alpha), s_M^R(\alpha)]$. In the α-plane representation, the boundary points for the type-2 membership matrices are computed as

$$a_i^R(x_j|\alpha) = \max\left(u_{ij}^{'L}, u_{ij}^{'R} \right), a_i^L(x_j|\alpha) = \min\left(u_{ij}^{'L}, u_{ij}^{'R} \right). \quad (32)$$

The new type-2 membership values are expressed as

$$a_i(x_j) = \bigcup_{\alpha \in [0,1]} \alpha / \left[a_i^L(x_j|\alpha), a_i^R(x_j|\alpha) \right]. \quad (33)$$

The type-2 membership function (a_i) of a pixel x_j in a cluster y_i is now expressed as

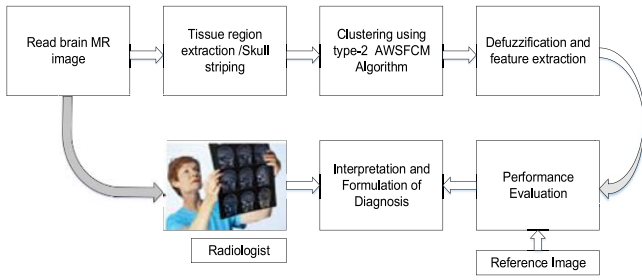$$a_i = \sum_{x_j \in X} a_i(x_j). \quad (34)$$

Fig. 2. Block diagram for the type-2 AWSFCM clustering approach for MR brain tissue segmentation.

Fig. 3. T1-w image. (a) Brain image. (b) Skull-striped brain-only image.

Initially, the cluster centers are randomly selected as practiced in the standard FCM. They are updated as

$$y_i = \sum_{j=1}^{N} w_{ij}\big(a_i(x_j)\big)^M x_j \bigg/ \sum_{j=1}^{N} w_{ij}\big(a_i(x_j)\big)^M \qquad (35)$$

where $w_{ij} = \|x_j - y_i\|$ represents the adaptive weights computed using the Euclidean distance between the data point x_j and the updated cluster center y_i. The concept of adaptive weights assigns the equidistant pixels to a single cluster by considering the distance of the pixel nearer to the expected decision boundary. A type-2 approach using the linguistic fuzzifier (M) in the given linguistic interval $[s_M^L(\alpha), s_M^R(\alpha)]$ for calculating the membership values and the cluster centers is found to be more accurate. Furthermore, this locates the cluster centers in more accurate locations than that of the standard FCM in the presence of noise and IIH.

The suggested AWSFCM approach may converge to some local minima. This is avoided by comparing the variations in the fitness function in succeeding iterative stages. The iteration ends when the minimum improvement between successive fitness function values is less than a predetermined error threshold. Defuzzification is used to allocate each pixel to a specific cluster as per its maximal membership value. The algorithm includes a new fitness function for clustering with adaptive weighted and spatial information of the neighboring pixels. The suggested fitness function J_{AWSFCM} is given as

$$J_{\text{AWSFCM}} = \sum_{j=1}^{N} \sum_{i=1}^{c} \big(a_i(x_j)\big)^M \|x_j - y_i\|^2. \qquad (36)$$

B. Flow Diagram

The flow diagram of the suggested model is presented in Fig. 2. Brain MR image reading, tissue region extraction or skull stripping, clustering using the algorithm, defuzzification and feature extraction, and performance evaluation are the main building blocks of the model. The selected volume of brain MR images is read from the BrainWeb/IBSR database for analysis.

The brain MR image contains the brain tissues and the nonbrain tissue regions as well. The nonbrain tissue regions are the skull bone, fat, etc. Therefore, in the tissue region segmentation stage, the brain-only portion is extracted after removing the nonbrain tissue regions. Now, the remaining tissue region

contains three major brain tissues, GM, WM, and CSF only. Fig. 3 shows the T1-w brain MR image and the brain-only region after removing the nonbrain tissue regions.

This process of removal of the skull bone and fat region is performed using the regional labeling and morphological operations as discussed in [35]. The next block is the clustering approach using the type-2 AWSFCM algorithm. As there are mainly three types of brain tissues present in the brain-only portion, the number of clusters is chosen three. Initially, the value for the fuzzifier is initialized in a linguistic interval. Using these interval linguistic values of the fuzzifier, the fuzzy value of the linguistic fuzzifier (M) is computed using (25). Furthermore, the cluster centers are randomly declared. The type-2 membership values are updated using (33), the cluster centers are updated using (35), and the fitness function is calculated using (36). It is optimized using the iterative conditional mode optimization algorithm. This approach assigns the equidistant pixels to a single cluster by assigning larger weights to the pixels close to the expected decision boundary. The adaptive spatial information derived from the neighborhood pixels enhances the noise performance of the proposed model.

The value of minimum improvement in the fitness function is taken as the stopping criterion. However, researchers can also consider the maximum number of iterations as an alternative criterion. At this stage, the given brain MR image is partitioned into three clusters. Each pixel is having three membership values. The principle of defuzzification is applied to obtain the tissue segments from the membership matrix. A pixel is assigned to a cluster where it is having the highest membership value. The pseudocode of the type-2 AWSFCM algorithm is given as follows.

C. Pseudocode of the Suggested Technique

Read the brain MR image.

Initialize number of clusters ($c = 3$), specify the value of the fuzzifier [$S_m^L = 1$ $S_m^R = 4$], assume maximum number of iterations ($l = 100$), assume error thresholds ($e_1 = 0.001, e_2 = 0.01$), $p = 2, q = 2$.

1) Abstract the brain portion stripping the skull portion.
2) Initialize the cluster centers randomly.
3) Initialize the linguistic interval values.
4) Calculate the linguistic fuzzifiers (M) using (25).
5) Calculate the partition membership value using (31).
   For iteration $i = 1, \ldots, l$ **do**
   a) Calculate the type-2 membership value using (33)
   b) Update the cluster centers using (35)
   c) Calculate the fitness function using (36)

This article has been accepted for inclusion in a future issue of this journal. Content is final as presented, with the exception of pagination.

MISHRO *et al.*: NOVEL TYPE-2 FUZZY *C*-MEANS CLUSTERING FOR BRAIN MR IMAGE SEGMENTATION 7

d) **If** minimum improvement is less than the error threshold e_1, then break the loop. **endIf**

e) **If** minimum improvement is less than the error threshold e_2, reduce the order of the filter. **endIf endFor**

6) Defuzzification of each cluster to obtain the tissue regions.

7) Extraction of the segmented brain tissue regions.

IV. RESULTS AND VALIDATIONS

The suggested type-2 AWSFCM algorithm is experimented with two sets of brain MR images. The first set contains eight volumes with 51 images each of the simulated brain MR images obtained from the BrainWeb [31] database. The second set contains one volume with 21 images of real brain MR image obtained from the IBSR [32] database. We simulated the model using MATLAB with core *i*-5 processor, 4-GB RAM. The effectiveness of the suggested method is compared with the standard FCM [21], AFCM [23], IIFCM [24], csFCM [25], FRFCM [26], DSFCM_N [27], IT2FCM [28], and GT2FCM [29] clustering algorithms. The performance of the model is validated using qualitative and quantitative analysis. The statistical analysis is also carried out to compare the results. A deeper insight into the analysis of results is provided in the following sections.

A. Simulated Brain MR Images

The ground truth for real brain MR images is usually not available, therefore it is not possible to assess the segmentation performance quantitatively. The simulated brain database [31] provides the discrete anatomical models for the tissue regions (GM, WM, and CSF). The discrete anatomical models of tissue regions with 0% noise and 0% IIH are considered as the reference image for the quantitative evaluation procedure. Here, the noise in the background of the simulated image follows the Rayleigh distribution and the signal region follows the Rician distribution. The percentage of noise indicates the deviation of intensity levels of the tissue regions from its actual values due to the white Gaussian noise. For instance, 5% of noise indicate the deviation of the tissue intensities by ± 5 from its actual values. From the literature, the maximum value of noise is found to be 9%, beyond which the quality of the image degrades up to mark. Similarly, a 20% level of IIH indicates an inhomogeneity in the range [0.90, 1.10] over the brain area. For other IIH levels, the field is linearly scaled (for instance, to a range [0.80, 1.20] for 40% level).

The evaluation of the model is accomplished with three volumes of T1-w, three volumes of T2-w, and three volumes of proton density (PD) brain MR images with different percentage of noise and IIH (for 1-mm slice thickness). Here, T1-w, T2-w, and PD brain MR images are the different modalities of the MR imaging technique with customizing the repetition and echo pulse sequences. The T1-w is generated from the RF-spoiled gradient recalled echo. In this modality, the CSF appears dark and GM appears darker than WM. The T2-w is the dual-echo spin-echo scan with late echo. In this modality, the CSF appears bright and GM appears brighter than WM. The PD is the dual-echo spin scan with early echo. The tissue region intensity distribution of the PD image is similar to the T2-w. However, the image in this modality appears brighter.

A typical volume of brain MR image contains 217 slices. It is observed that the distinguishable tissue regions are mostly found in the near middle slices of the volume. These slices are clinically normal and contain distinguishable portions of all the three tissue regions. So, a sample of 51 slices (slice no. 50–100) are selected for the evaluation procedure. The MR brain tissue segmentation is performed using the standard FCM, AFCM, IIFCM, csFCM, FRFCM, DSFCM_N, IT2FCM, and GT2FCM clustering algorithms and compared with our algorithm.

Qualitative Evaluation: The qualitative analysis provides the visual representation of the clustering approaches. The simulated T1-w brain MR images of size 181×181 are read from the BrainWeb dataset. Fig. 4 presents the segmented results of the T1-w brain MR image using different methods. Fig. 4 (first row) shows the discrete anatomical model of tissue regions and the brain-only portion with 7% noise and 20% IIH at 1-mm slice thickness (reference images). The remaining rows are the segmented images with FCM, AFCM, IIFCM, csFCM, FRFCM, DSFCM_N, IT2FCM, GT2FCM, and our model, respectively. Fig. 4 shows that with higher values of noise and IIH, the FCM and its modifications are incompetent to segment the tissue regions correctly. The presence of noise is easily identified and IIH still persists. It is observed that the output image obtained using FRFCM is having a poor contrast due to which the tissue regions are not distinguishable.

Even though the output obtained with DSFCM_N, IT2FCM, and GT2FCM methods is having a better contrast, the noise is not removed completely. Furthermore, the tissue regions are also not distinguishable. The suggested type-2 AWSFCM model gives the segmented tissue regions more accurately with minimum residual noise.

Fig. 4 (last row) shows the GM, WM, and CSF tissue regions of the subject image obtained using the proposed technique. The visual comparison of the resulting images using the algorithm appears to be more similar to the reference image. However, the actual performance appraisal is defined using the quantitative analysis. The absence of nonintersecting tissue regions demonstrates the superiority of the proposed model over the other methods even in the presence of higher values of noise and IIH.

It is observed that images obtained with other methods have intersecting tissue regions. For instance, images in AFCM and IIFCM clearly show the traces of noise, whereas the image obtained with our method is free from noise. As mentioned above, the earlier methods use standard FCM. The idea of type-2 FCM followed by the introduction of adaptive weighted spatial information in the fitness function solves the problem of equidistant pixels and accurately determines the cluster centers. This results in a noise-free output image with nonintersecting tissue regions. It is also observed that there is an improvement in the output image quality as we proceed from FCM to AWSFCM (Fig. 4). This shows the gradual improvement in the research and development of the standard FCM
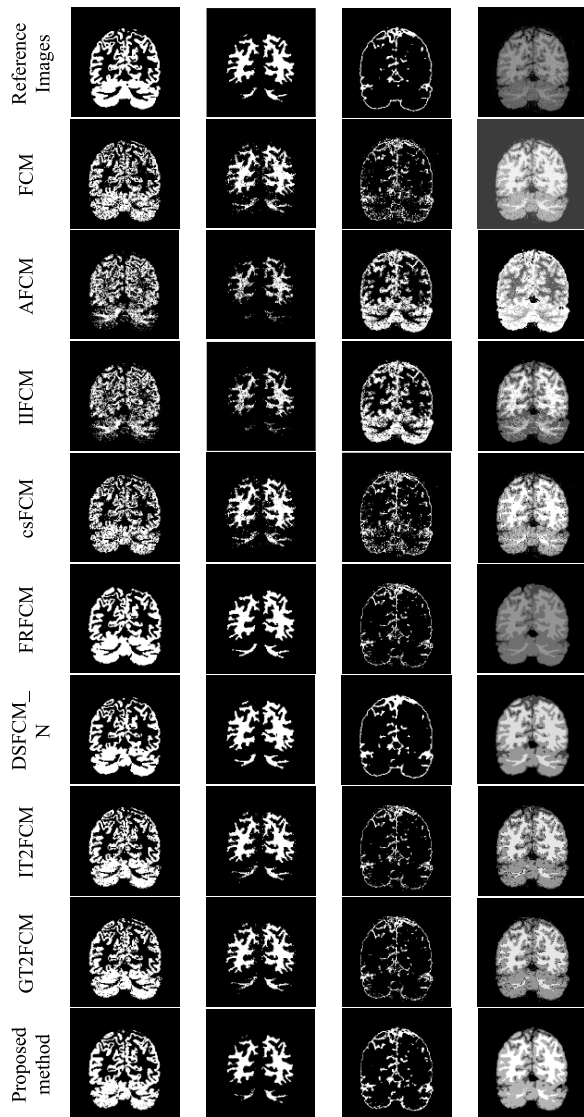
Fig. 4. Segmentation results with T1-w brain MR images (slice-60) using different methods.
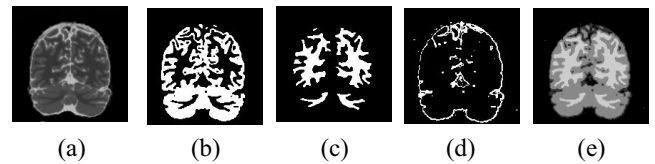

Fig. 5. Segmentation results with T2-w image. (a) Brain-only portion. (b)–(d) GM, WM, and CSF regions, respectively. (e) Segmented image using the AWSFCM clustering approach.
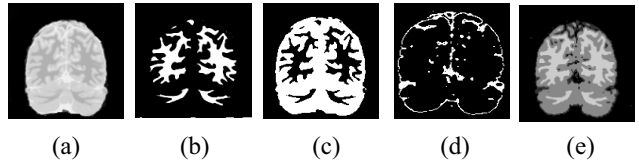

Fig. 6. Segmentation results with PD image. (a) Brain-only image. (b)–(d) Corresponding GM, WM, and CSF regions, respectively. (e) Proposed method output.

clustering technique over the years. Finally, our investigation adds more strength to the subsequent developments for which the algorithm is more robust toward noise and IIH. It depicts the significant improvement in the visual quality. The reason is the addition of weighted spatial information together with the type-2 fuzzy membership function.

Fig. 5 displays the qualitative analysis of the proposed algorithm using T2-w brain MR images. Fig. 5(a) presents the brain-only portion, Fig. 5(b)–(d) is the corresponding extracted tissue regions for GM, WM, and CSF, respectively, and Fig. 5(e) shows the segmented brain MR image using the AWSFCM clustering approach.

The qualitative analysis of the suggested model using the PD brain MR image is shown in Fig. 6. Fig. 6(a) shows the brain MR image, Fig. 6(b)–(d) shows the extracted tissue regions for GM, WM, and CSF regions, respectively, and Fig. 6(e) shows the segmented image using the suggested type-2 AWSFCM algorithm. The claim is further supported by the quantitative evaluation which provides deep insights into the

proposed work. The location and intensity levels of the cluster centers play a crucial role in differentiating the three brain tissue regions.

The introduction of the type-2 FCM fitness function leads to more accurate cluster centers. The suggested model is successful in identifying accurate cluster centers because the use of spatial information in the newly proposed type-2 FCM fitness function localizes the cluster centers. The expected decision boundary selection becomes easier. Therefore, the cluster centers are converging more accurately toward their actual values. The presence of IIH delocalizes the cluster centers. The occurrence of noise results in inaccurate cluster centers. However, the use of (35) for updating the cluster centers is found well suited under IIH and noisy conditions. Because the weighted mean is computed using the initial cluster center and the data points. It is interesting to reiterate that y_i is computed using type-2 fuzzy membership values. Note that (33) uses the new membership values that resulted in the addition of spatial information. The equidistant pixel problem is resolved by introducing a weight factor that assigns the pixels to its expected decision boundary. The possible reason could be the change of membership function values from 0.5 to a higher value. The addition of spatial information into the membership values helps in reducing the noise. The improved accuracy of the cluster centers, because of type-2 AWSFCM, results in a nonintersecting brain tissue region.

Quantitative Evaluation: The quantitative evaluation provides the numerical significance of a model. The cluster validation indices [36] and the segmentation validation indices [25], [37], [38] are used for quantitative evaluation. The details of the performance indices are available in the corresponding literature.

Partition Coefficient (V_{PC}): This is an indicator of the degree of fuzzy partition among the clusters. The optimum value of this validation metric is 1 [36]. This is formulated as follows:

$$V_{PC} = \sum_{i=1}^{c} \sum_{j=1}^{N} u_{ij}^2 \bigg/ N. \tag{37}$$

This article has been accepted for inclusion in a future issue of this journal. Content is final as presented, with the exception of pagination.

MISHRO *et al.*: NOVEL TYPE-2 FUZZY *C*-MEANS CLUSTERING FOR BRAIN MR IMAGE SEGMENTATION

9

Classification Entropy (V_{CE}): This cluster validation parameter indicates the degree of miss classification among the clusters. The optimum value of this parameter is 0 [36]. This is formulated as follows:

$$V_{CE} = \left(-\sum_{i=1}^{c} \sum_{j=1}^{N} \left[u_{ij} \log u_{ij} \right] \right) / N. \tag{38}$$

Jaccard Coefficient (JC): JC is a segmentation validation index. This is defined as the ratio of intersection over union [37] of the segmented image and the reference image. The parameter is calculated with the following expression:

$$JC(A, B) = |A \cap B| / |A \cup B|. \tag{39}$$

Dice Similarity Index (DSI): DSI is an efficient segmentation validation index that finds the similarity between the segmented results and the reference image [38]. The index is computed as

$$DSI(A, B) = \frac{1}{c} \sum_{i=1}^{c} (2|A_i \cap B_i|) / |A_i| + |B_i| \tag{40}$$

where A_i and B_i are the sets of pixels from the segmented image and reference image, respectively [25].

Segmentation Accuracy (SA): The segmentation validation index SA is expressed as the addition of the rightly classified pixels out of the total number of pixels of the segmented image [25]. The SA is calculated as follows:

$$SA = \sum_{k=1}^{N} \text{card}(A_k \cap B_k) \bigg/ \sum_{k=1}^{N} \text{card}(B_k) \tag{41}$$

where N is the total number of pixels in a cluster.

Tissue SA (TSA): The TSA is an indicator of rightly classified pixels out of the total number of pixels in an image. The TSA is calculated as follows:

$$TSA = 2N_{CTK} / (N_{CITK} + N_{GTK}) \tag{42}$$

where N_{CTK} is the number rightly assigned pixels with a given method, N_{CITK} is the total number of pixels contained in the image, and N_{GTK} is the number of pixels belonging to the reference image [25]. The optimum value of JC, DSI, SA, and TSA is "1," values closer to 1 are better.

Table I shows the comparison of V_{PC} and V_{CE} using the suggested model compared to other approaches. The values shown here are the average values of the 51 slices. The cluster validation index V_{PC} indicates the fuzzy partition. The higher values in Table I indicate less intersection of the tissue regions. The proposed technique shows 3%–7% improvement in the segmented tissue regions. The cluster validation index V_{CE} is an indicator of homogeneity in the samples. The value of $V_{CE} = 0$ indicates a complete homogeneous classification. The suggested technique results in the values of V_{CE} close to 0 as shown in Table I. This indicates the classified tissue regions are more homogeneous in comparison to the other discussed techniques. It is evident from the literature that these indices involve only the membership values. The membership matrix plays a crucial role in defining these indices. The role of a pattern having a lower membership value is relatively smaller in type-2 fuzzy systems. For this reason, the membership values obtained with our method better represent typicality. For instance, the V_{PC} value obtained with FCM is 0.8864, whereas it is 0.9659 using our method. There is an increase in its value as we go on improvising the standard FCM by adding spatial information. A consistent improvement in the values of the indices with an increase in noise and IIH strengthens our claim for a better method for brain tissue segmentation. A similar trend is also observed for V_{CE}.

Table I also shows the quantitative analysis of DSI, JC, SA, and TSA values. The segmentation evaluation indices are computed with respect to the corresponding reference images. The higher values of the indices indicate a higher degree of similarity between the reference image and the output. The best values are marked in bold. It is witnessed that the suggested procedure outperforms the other techniques. The uncertainty in determining the cluster centers is considerably reduced. The segmentation validation indices computed above are sensitive to the misplacement of the segmentation label. Any intersecting segments in the output images will worsen the values. The equidistant pixels will pose a challenge in evaluating the values.

Furthermore, inaccurate cluster centers will affect the robustness of the method. For instance, the SA value obtained with FCM in Table I is 0.8499, whereas it is 0.8654 with our method. A better value is achieved with our method as the probability of overlap among the tissue regions is decreased. The equidistant pixels are assigned to a single cluster only using a type-2 fuzzy membership matrix and the spatial information. The adaptive weights introduced in the fitness function improve the cluster centers and prevents any intersection between the tissue boundaries. A similar behavior is observed while computing TSA, DSI, and JC.

Fig. 7 presents the cluster validation parameters using the proposed algorithm in comparison to the standard FCM, AFCM, IIFCM, csFCM, FRFCM, DSFCM_N, IT2FCM, and GT2FCM algorithms. It is observed in Fig. 7(a) that the partition coefficient values are maximum in our case. Fortunately, the performance is better for all slices. From Fig. 7(b), it is seen that the classification entropy has the lowest value, which is desirable. Interestingly, it also happened with all slices. Fig. 8(a)–(d) depicts the variation of the performance indices for the three tissue regions (GM, WM, and CSF) utilizing different clustering approaches. This comparison is performed with 51 slices of MR brain image with 7% of noise and 20% of IIH. The graphs plotted here show the stable and superior performance of the suggested approach in comparison with the existing standard procedures. More is the value of these indices, better is the performance. These values are maximum in all cases for all slices [as observed in Fig. 8(a)–(d)].

Table II presents the quantitative analysis of the AWSFCM model in comparison with the existing standard methods using T2-w brain MR images. This table displays the average values of all the three tissue regions for both the cluster validation indices and the segmentation validation indices. The boldfaced numerical values in the tables indicate the best results which are obtained with the proposed model.

TABLE I
COMPARISON OF AVERAGE DSI, JC, SA, TSA, V_{PC}, AND V_{CE} VALUES WITH T1-W BRAIN MR IMAGES (COMPUTED OVER 51 SLICES)

Image Volume	Method	DSI			JC			SA			TSA			V_{PC}	V_{CE}
		CSF	GM	WM	CSF	GM	WM	CSF	GM	WM	CSF	GM	WM		
3% Noise + 0%IIH	FCM	0.6767	0.8734	0.8591	0.5095	0.7624	0.7516	0.8498	0.8039	0.8667	0.9025	0.9264	0.8713	0.8864	0.2224
	AFCM	0.6724	0.8735	0.8515	0.5101	0.7721	0.7611	0.8524	0.8052	0.8628	0.9064	0.9242	0.8714	0.8956	0.2019
	IIFCM	0.6814	0.8814	0.8611	0.5144	0.7601	0.7548	0.8541	0.8121	0.8699	0.9113	0.9282	0.8826	0.9015	0.1814
	csFCM	0.6899	0.8825	0.8621	0.5289	0.7791	0.7614	0.8589	0.8124	0.8859	0.9137	0.9291	0.8841	0.9124	0.1064
	FRFCM	0.6708	0.8574	0.8498	0.5051	0.7606	0.7516	0.8332	0.7988	0.8732	0.8738	0.8993	0.8682	0.9088	0.1124
	DSFCM_N	0.6745	0.8648	0.8541	0.5159	0.7754	0.7642	0.8584	0.8141	0.8647	0.9087	0.9154	0.8749	0.9124	0.1039
	IT2FCM	0.6715	0.8729	0.8657	0.5208	0.7724	0.7649	0.8474	0.8109	0.8707	0.8810	0.9042	0.8788	0.9237	0.0960
	GT2FCM	0.6824	0.8867	0.8701	**0.5386**	0.7778	0.7687	0.8612	**0.8284**	0.8845	0.8914	0.9145	0.8746	0.9328	0.0837
	AWSFCM	**0.7035**	**0.9035**	**0.8824**	0.5379	**0.7889**	0.7826	0.8654	0.8265	**0.9022**	**0.9347**	**0.9382**	**0.8924**	**0.9659**	**0.0564**
3% Noise + 20%IIH	FCM	0.6633	0.8526	0.8345	0.4875	0.7589	0.7426	0.8056	0.7845	0.8455	0.8541	0.9127	0.8546	0.8856	0.2211
	AFCM	0.6688	0.8588	0.8344	0.4915	0.7541	0.7499	0.8019	0.7901	0.8488	0.8595	0.9155	0.8511	0.8894	0.2024
	IIFCM	0.6712	0.8629	0.8426	0.4955	0.7628	0.7514	0.8099	0.8011	0.8521	0.8562	0.9186	0.8642	0.9024	0.1846
	csFCM	0.6659	0.8647	0.8547	0.5099	0.7701	0.7552	0.8115	0.8056	0.8726	0.8645	0.9248	0.8757	0.9129	0.1112
	FRFCM	0.6524	0.8417	0.8239	0.4751	0.7610	0.7414	0.7968	0.7857	0.8568	0.8579	0.9099	0.8657	0.9002	0.1742
	DSFCM_N	0.6748	0.8577	0.8341	0.4891	0.7657	0.7489	0.8018	0.7941	0.8501	0.8585	0.9119	0.8654	0.9185	0.1524
	IT2FCM	0.6641	0.8574	0.8381	0.4799	0.7712	0.7521	0.8141	0.8010	0.8659	0.8601	0.9143	0.8724	0.9241	0.1037
	GT2FCM	0.6722	0.8675	0.8514	0.4984	**0.7891**	0.7549	0.8188	0.8048	0.8745	**0.8781**	0.9244	0.8912	0.9347	0.0914
	AWSFCM	**0.6925**	**0.8956**	**0.8659**	**0.5201**	0.7871	**0.7609**	**0.8329**	0.8124	**0.8958**	0.8759	**0.9311**	**0.9077**	**0.9598**	**0.0645**
5% Noise + 0%IIH	FCM	0.6425	0.8397	0.8156	0.4821	0.7356	0.7254	0.7864	0.7598	0.8165	0.8349	0.9087	0.8342	0.8745	0.2219
	AFCM	0.6469	0.8421	0.8124	0.4812	0.7426	0.7289	0.7948	0.7526	0.8122	0.8459	0.9013	0.8325	0.8845	0.1846
	IIFCM	0.6548	0.8477	0.8241	0.4932	0.7451	0.7315	0.8059	0.7677	0.8234	0.8412	0.9048	0.8468	0.8962	0.1794
	csFCM	0.6557	0.8547	0.8364	0.5246	0.7423	0.7484	0.8124	0.7749	0.8465	0.8467	0.9025	0.8457	0.9034	0.1211
	FRFCM	0.6472	0.8446	0.8224	0.5154	0.7458	0.7288	0.7948	0.7470	0.8065	0.8251	0.8810	0.8220	0.9058	0.1526
	DSFCM_N	0.6549	0.8474	0.8181	0.4908	0.7437	0.7263	0.7928	0.7575	0.8167	0.8416	0.9032	0.8342	0.9124	0.1132
	IT2FCM	0.6565	0.8541	0.8222	0.5147	0.7455	0.7342	0.8010	0.7721	0.8214	0.8411	0.8941	0.8421	0.9264	0.0981
	GT2FCM	0.6621	0.8589	0.8311	0.5199	0.7521	0.7433	0.8134	0.7714	0.8323	0.8546	0.9059	0.8544	0.9288	0.0721
	AWSFCM	**0.6734**	**0.8694**	**0.8419**	**0.5329**	**0.7625**	**0.7562**	**0.8254**	**0.8026**	**0.8589**	**0.8649**	**0.9134**	**0.8749**	**0.9468**	**0.0644**
5% Noise + 20%IIH	FCM	0.6215	0.8026	0.7945	0.4687	0.7254	0.7244	0.7789	0.7249	0.7899	0.8267	0.8725	0.8144	0.8645	0.2301
	AFCM	0.6228	0.8132	0.8011	0.4729	0.7364	0.7311	0.7958	0.7285	0.7901	0.8248	0.8755	0.8178	0.9065	0.1768
	IIFCM	0.6318	0.8166	0.8035	0.4736	0.7326	0.7349	0.8051	0.7311	0.8054	0.8298	0.8814	0.8139	0.9055	0.1524
	csFCM	0.6482	0.8299	0.8214	0.5002	0.7359	0.7221	0.8029	0.7359	0.8165	0.8399	0.8723	0.8266	0.9144	0.1246
	FRFCM	0.6214	0.8099	0.8006	0.4671	0.7120	0.7160	0.7617	0.7189	0.7879	0.8155	0.8678	0.8047	0.9241	0.1532
	DSFCM_N	0.6257	0.8127	0.8024	0.4757	0.7324	0.7342	0.7988	0.7247	0.7981	0.8224	0.8742	0.8140	0.9346	0.1127
	IT2FCM	0.6345	0.8144	0.8059	0.4859	0.7243	0.7246	0.7985	0.7345	0.8042	0.8297	0.8868	0.8059	0.9214	0.1062
	GT2FCM	0.6422	0.8211	0.8142	0.5084	0.7312	0.7319	0.8047	0.7526	0.8167	0.8326	0.8838	0.8236	0.9292	0.0834
	AWSFCM	**0.6724**	**0.8364**	**0.8367**	**0.5168**	**0.7425**	**0.7438**	**0.8199**	**0.7749**	**0.8322**	**0.8514**	**0.8936**	**0.8455**	**0.9411**	**0.0688**
7% Noise + 0%IIH	FCM	0.6154	0.7905	0.7849	0.4568	0.7211	0.7124	0.7721	0.7244	0.7749	0.8127	0.8596	0.8019	0.8657	0.2341
	AFCM	0.6206	0.8010	0.7824	0.4599	0.7266	0.7214	0.7814	0.7301	0.7788	0.8146	0.8601	0.8065	0.8725	0.1844
	IIFCM	0.6288	0.8112	0.7894	0.4627	0.7257	0.7286	0.7892	0.7419	0.7812	0.8157	0.8628	0.8125	0.8895	0.1728
	csFCM	0.6312	0.8116	0.7849	0.4921	0.7299	0.7212	0.7789	0.7356	0.8011	0.8267	0.8617	0.8322	0.9188	0.1349
	FRFCM	0.6221	0.7850	0.7735	0.4671	0.7097	0.7041	0.7641	0.7267	0.7681	0.8046	0.8457	0.7941	0.9017	0.1221
	DSFCM_N	0.6363	0.8080	0.7842	0.4542	0.7235	0.7248	0.7759	0.7342	0.7757	0.8124	0.8583	0.8109	0.9145	0.1044
	IT2FCM	0.6323	0.7958	0.7952	0.4811	0.7118	0.7088	0.7741	0.7321	0.7844	0.8222	0.8549	0.8246	0.9241	0.0936
	GT2FCM	0.6415	0.8041	0.8023	0.5014	0.7227	0.7141	0.7884	0.7436	0.8037	0.8301	0.8711	0.8355	0.9287	0.0872
	AWSFCM	**0.6624**	**0.8185**	**0.8243**	**0.5077**	**0.7324**	**0.7328**	**0.8099**	**0.7548**	**0.8299**	**0.8469**	**0.8824**	**0.8459**	**0.9377**	**0.0712**
7% Noise + 20%IIH	FCM	0.6124	0.7854	0.7748	0.4428	0.7024	0.7085	0.7658	0.7165	0.7629	0.8349	0.8401	0.7945	0.8647	0.2345
	AFCM	0.6261	0.7812	0.7758	0.4568	0.7082	0.7112	0.7712	0.7122	0.7645	0.8355	0.8455	0.7984	0.8718	0.1833
	IIFCM	0.6258	0.7856	0.7806	0.4681	0.7124	0.7184	0.7649	0.7185	0.7718	0.8368	0.8484	0.8064	0.8749	0.1742
	csFCM	0.6356	0.7814	0.7719	0.4711	0.7199	0.7154	0.7789	0.7256	0.7795	0.8434	0.8569	0.8124	0.8841	0.1346
	FRFCM	0.6214	0.7842	0.7841	0.4524	0.7019	0.7031	0.7648	0.7137	0.7612	0.8251	0.8427	0.8019	0.8746	0.1237
	DSFCM_N	0.6257	0.7818	0.7751	0.4528	0.7042	0.7144	0.7652	0.7168	0.7683	0.8328	0.8453	0.8007	0.8837	0.1472
	IT2FCM	0.6308	0.7881	0.7954	0.4627	0.7085	0.7084	0.7734	0.7181	0.7701	0.8342	0.8524	0.8155	0.8952	0.1059
	GT2FCM	0.6475	0.7921	0.8061	0.4717	0.7142	0.7175	0.7787	0.7256	0.7810	0.8383	0.8566	0.8192	0.9037	0.0879
	AWSFCM	**0.6584**	**0.8099**	**0.8134**	**0.4857**	**0.7264**	**0.7214**	**0.7849**	**0.7364**	**0.7829**	**0.8569**	**0.8719**	**0.8367**	**0.9310**	**0.0756**

Table III displays the quantitative analysis of the suggested model in comparison with the prevailing standard methods using PD brain MR images. This table presents the average values of all the three tissue regions for both the cluster validation indices and the segmentation validation indices.

B. Real Brain MR Images

The validation of the suggested model with the real brain MR image is accomplished with one volume of clinically normal images obtained from the "20 Normals_T1" dataset of the IBSR database. From this, 21 number of selected images are experimented to validate the model. The IBSR database provides manually segmented images for the quantitative analysis.

Fig. 9 presents the qualitative analysis of the proposed model with a real brain MR image obtained from the IBSR database. Fig. 9(a) shows the real brain MR image, Fig. 9(b)–(d) is the extracted tissue regions for GM, WM, and CSF, respectively, and Fig. 9(e) shows the segmented image, utilizing the proposed algorithm. The nonintersecting regions
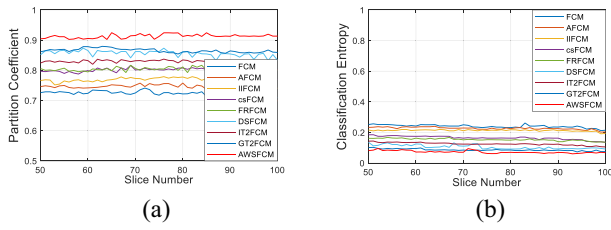
This article has been accepted for inclusion in a future issue of this journal. Content is final as presented, with the exception of pagination.

MISHRO *et al.*: NOVEL TYPE-2 FUZZY *C*-MEANS CLUSTERING FOR BRAIN MR IMAGE SEGMENTATION 11

Fig. 7. Graphical representation of cluster validation indices (for 51-slices of T1-w brain MR image) having 7% noise and 20% IIH. (a) Partition Coefficient. (b) Classification Entropy.
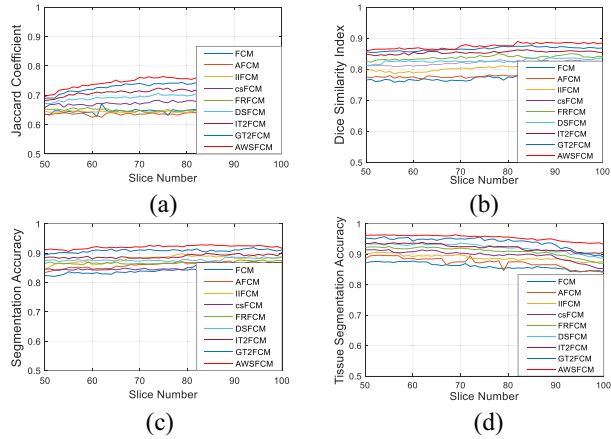

Fig. 8. Graphical representation of segmentation evaluation indices (using 51 slices of T1-w brain MR image) bearing 7% noise and 20% IIH. (a) JC. (b) DSI. (c) SA. (d) TSA.
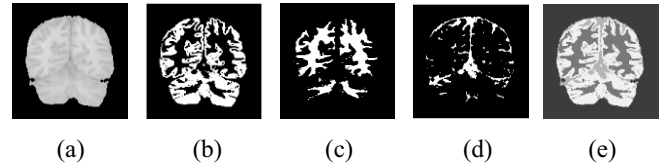

Fig. 9. Segmentation results with real brain MR image. (a) Real brain-only MR image. (b) Segmented image. (c)–(e) Corresponding GM, WM, and CSF regions, respectively, using the AWSFCM clustering algorithm.

TABLE II
COMPARISON OF PERFORMANCE INDICES WITH T2-W
MR BRAIN IMAGES

Method	V_{PC}	V_{CE}	JC	DSI	SA	TSA
FCM	0.7801	0.2216	0.6911	0.7518	0.7789	0.8928
AFCM	0.7902	0.2019	0.7079	0.7644	0.7928	0.9184
IIFCM	0.8114	0.1824	0.7099	0.7727	0.8014	0.9226
csFCM	0.8234	0.1242	0.7249	0.7899	0.8167	0.9344
FRFCM	0.8219	0.1811	0.7084	0.7645	0.8088	0.9011
DSFCM_N	0.8057	0.1610	0.7028	0.7681	0.8017	0.9132
IT2FCM	0.8423	0.1257	0.7225	0.7714	0.8080	0.9127
GT2FCM	0.8547	0.1001	0.7289	0.7923	0.8114	0.9289
AWSFCM	**0.8747**	**0.0824**	**0.7301**	**0.8381**	**0.8227**	**0.9542**

TABLE III
COMPARISON OF PERFORMANCE INDICES WITH PD MR BRAIN IMAGES

Method	V_{PC}	V_{CE}	JC	DSI	SA	TSA
FCM	0.7615	0.2332	0.6748	0.7544	0.7727	0.8638
AFCM	0.7754	0.2015	0.6859	0.7529	0.7846	0.9012
IIFCM	0.7814	0.1818	0.6894	0.7646	0.7942	0.9055
csFCM	0.7922	0.1746	0.6925	0.7734	0.8023	0.9125
FRFCM	0.7749	0.1688	0.6849	0.7655	0.7869	0.9090
DSFCM_N	0.7814	0.1601	0.6827	0.7621	0.7824	0.9042
IT2FCM	0.7872	0.1507	0.6972	0.7782	0.8057	0.9146
GT2FCM	0.8012	0.1349	0.7014	0.7851	0.8201	0.9258
AWSFCM	**0.8327**	**0.1025**	**0.7266**	**0.7985**	**0.8356**	**0.9429**

TABLE IV
COMPARISON OF PERFORMANCE INDICES WITH REAL
BRAIN MR IMAGES

Method	V_{PC}	V_{CE}	JC	DSI	SA	TSA
FCM	0.7931	0.2021	0.7234	0.7722	0.8012	0.8532
AFCM	0.8126	0.1843	0.7325	0.7861	0.8112	0.8743
IIFCM	0.8214	0.1643	0.7344	0.7952	0.8322	0.8811
csFCM	0.8342	0.1011	0.7582	0.8102	0.8512	0.8902
FRFCM	0.8149	0.1123	0.7641	0.8025	0.8379	0.8756
DSFCM_N	0.8187	0.1251	0.7324	0.8027	0.8277	0.8834
IT2FCM	0.8349	0.1024	0.7564	0.8129	0.8421	0.8864
GT2FCM	0.8516	0.0842	0.7622	0.8217	0.8499	0.8991
AWSFCM	**0.9038**	**0.0475**	**0.7741**	**0.8381**	**0.8726**	**0.9148**

TABLE V
STATISTICAL ANALYSIS OF AWSFCM WITH OTHER METHODS USING
THE FRIEDMAN TEST

Method	V_{PC}	V_{CE}	JC	DSI	SA	TSA
FCM	0.0001	0.0001	0.0332	0.0113	0.0358	0.0361
AFCM	0.0001	0.0001	0.0391	0.0153	0.0131	0.0260
IIFCM	0.0001	0.0001	0.0250	0.0272	0.0167	0.0285
csFCM	0.0001	0.0001	0.0233	0.0223	0.0254	0.0259
FRFCM	0.0001	0.0001	0.0224	0.0229	0.0264	0.0281
DSFCM_N	0.0001	0.0001	0.0241	0.0247	0.0259	0.0267
IT2FCM	0.0001	0.0001	0.0334	0.0334	0.0315	0.0304
GT2FCM	0.0031	0.0011	0.0351	0.0333	0.0289	0.0292

TABLE VI
EXECUTION TIME ANALYSIS OF AWSFCM WITH OTHER METHODS

Method	Computational Complexity	Running Time (s)
FCM	$O(I\,n\,c^2)$	10.36
FRFCM	$O(I\,(w^2 + n\,c))$	5.68
IT2FCM	$O(I\,(2\,n\,c^2 + n\,c))$	9.73
GT2FCM	$O(I\,K\,(2\,n\,c^2 + n\,c))$	18.28
AWSFCM	$O(I\,K\,(w^2 + 2\,n\,c))$	9.36

in the figure indicate that the tissue regions are segmented more accurately with the insignificant residual noise.

Table IV presents the quantitative analysis of the proposed model utilizing real brain MR images (IBSR database). The segmentation evaluation indices are computed using the segmented image and the manually segmented image provided in the database. Table IV displays the average values of all the three tissue regions for both the cluster validation indices and the segmentation validation indices. The boldfaced numerical values indicate the best results which are obtained with our model.

The Friedman test [39] is performed on T1-w brain MR images from the BrainWeb database only. Table V shows the *p*-values on all the cluster validation and segmentation evaluation indices with a significance level of 0.05 between the proposed type-2 AWSFCM method and the other approaches. A similar statistical result is also obtained with T2-w and PD brain images.

Execution time is a measure to justify the computational effectiveness of a particular method. It depends upon the number of data points (n), number of clusters to be classified (c), filtering window size (w), the number of training iterations (I), number of α-planes (K) (in GT2FCM), and the work station configuration.

Table VI shows a comparative analysis of computational complexity and execution time analysis for different methods. The execution time is computed for a dataset of T1-w brain MR image at 7% noise and 20% IIH. The running time is calculated for $c = 3$, 10α-planes ($K = 10$), $n = 181 \times 181$, and the window size (w) = 5×5. The proposed method is faster than GT2FCM because the computation of centroids is not required. The final cluster centers are obtained by updating the type-2 membership values using the fuzzy linguistic fuzzifier.

V. CONCLUSION

Here, a type-2 AWSFCM clustering algorithm is introduced for brain MR tissue segmentation. The proposed algorithm offers a solution to the problem of equidistant pixels, assigning them to a single cluster by providing greater weights to the pixel closer to the expected decision boundary. The spatial information of the neighboring pixels is attained using the adaptive Gaussian filter, where the order of the filter decreases with the convergence of the algorithm to the final cluster centers. A type-2 approach for computation of the membership values and the cluster centers ensures a more accurate location of the cluster centers compared to the standard FCM clustering technique, in the presence of noise and IIH. Furthermore, the fuzzy value of the linguistic fuzzifier (M) obtained using the α-plane representation results in more accurate cluster centers. The qualitative and quantitative segmentation evaluation indices indicate that the proposed model outperforms the standard FCM, AFCM, IIFCM, csFCM, FRFCM, DSFCM_N, IT2FCM, and GT2FCM clustering approaches. This may set a new path in the area of brain MR tissue segmentation. The proposed approach is tested using healthy brain images. However, a test with images containing lesions may be taken up in the future.

REFERENCES

[1] S. Hussein *et al.*, "Automatic segmentation and quantification of white and brown adipose tissues from PET/CT scans," *IEEE Trans. Med. Imag.*, vol. 36, no. 3, pp. 734–744, Mar. 2017.

[2] M. Hajiaghayi, E. M. Groves, H. Jafarkhani, and A. Kheradvar, "A 3-D active contour method for automated segmentation of the left ventricle from magnetic resonance images," *IEEE Trans. Biomed. Eng.*, vol. 64, no. 1, pp. 134–144, Jan. 2017.

[3] L. Chen, C. L. P. Chen, and M. Lu, "A multiple-kernel fuzzy C-means algorithm for image segmentation," *IEEE Trans. Syst., Man, Cybern. B, Cybern.*, vol. 41, no. 5, pp. 1263–1274, Oct. 2011.

[4] S. Balla-Arabe, X. Gao, and B. Wang, "A fast and robust level set method for image segmentation using fuzzy clustering and lattice Boltzmann method," *IEEE Trans. Cybern.*, vol. 43, no. 3, pp. 910–920, Jun. 2013.

[5] Y. Kong, Y. Deng, and Q. Dai, "Discriminative clustering and feature selection for brain MRI segmentation," *IEEE Signal Process. Lett.*, vol. 22, no. 5, pp. 573–577, May 2015.

[6] A. Demirhan, M. Törü, and Ý. Güler, "Segmentation of tumor and EDEMA along with healthy tissues of brain using wavelets and neural networks," *IEEE J. Biomed. Health Informat.*, vol. 19, no. 4, pp. 1451–1458, Jul. 2015.

[7] Z. Ji, Y. Xia, Q. Sun, Q. Chen, D. Xia, and D. D. Feng, "Fuzzy local Gaussian mixture model for brain MR image segmentation," *IEEE Trans. Inf. Technol. Biomed.*, vol. 16, no. 3, pp. 339–347, May 2012.

[8] S.-L. Jui, C. Lin, H. Guan, A. Abraham, A. E. Hassanien, and K. Xiao, "Fuzzy C-means with wavelet filtration for MR image segmentation," in *Proc. 6th World Congr. Nat. Biol. Inspired Comput. (NaBIC)*, 2014, pp. 12–16.

[9] S. Roy *et al.*, "Subject-specific sparse dictionary learning for atlas-based brain MRI segmentation," *IEEE J. Biomed. Health Informat.*, vol. 19, no. 5, pp. 1598–1609, Sep. 2015.

[10] P. Moeskops *et al.*, "Automatic segmentation of MR brain images with a convolutional neural network," *IEEE Trans. Med. Imag.*, vol. 35, no. 5, pp. 1252–1261, May 2016.

[11] A. Banerjee and P. Maji, "Rough sets and stomped normal distribution for simultaneous segmentation and bias field correction in brain MR images," *IEEE Trans. Image Process.*, vol. 24, no. 12, pp. 5764–5776, Dec. 2015.

[12] A. Hamamci, N. Kucuk, K. Karaman, K. Engin, and G. Unal, "Tumor-cut: Segmentation of brain tumors on contrast enhanced MR images for radiosurgery applications," *IEEE Trans. Med. Imag.*, vol. 31, no. 3, pp. 790–804, Mar. 2012.

[13] A. Khademi, A. Venetsanopoulos, and A. R. Moody, "Robust white matter lesion segmentation in FLAIR MRI," *IEEE Trans. Biomed. Eng.*, vol. 59, no. 3, pp. 860–871, Mar. 2012.

[14] H. Chang *et al.*, "A new variational method for bias correction and its applications to rodent brain extraction," *IEEE Trans. Med. Imag.*, vol. 36, no. 3, pp. 721–733, Mar. 2017.

[15] X. Bai, Y. Zhang, H. Liu, and Z. Chen, "Similarity measure-based possibilistic FCM with label information for brain MRI segmentation," *IEEE Trans. Cybern.*, vol. 49, no. 7, pp. 2618–2630, Jul. 2019.

[16] L. Dora, S. Agrawal, R. Panda, and A. Abraham, "State-of-the-art methods for brain tissue segmentation: A review," *IEEE Rev. Biomed. Eng.*, vol. 10, pp. 235–249, Jun. 2017.

[17] J. C. Bezdek, E. Robert, and F. William, "FCM: The fuzzy C-means clustering algorithm," *Comput. Geosci.*, vol. 10, nos. 2–3, pp. 191–203, 1984.

[18] M. N. Ahmed, M. S. Yamany, N. Mohamed, A. A. Farag, and T. Moriarty, "A modified fuzzy C-means algorithm for bias field estimation and segmentation of MRI data," *IEEE Trans. Med. Imag.*, vol. 21, no. 3, pp. 193–199, Mar. 2002.

[19] N. A. Mohamed, *Modified Fuzzy C-Mean Algorithm for Medical Image Segmentation*, Comput. Vis. Image Process. Lab., Waterloo, ON, Canada, 1999.

[20] A. W. C. Liew and H. Yan, "An adaptive spatial fuzzy clustering algorithm for 3-D MR image segmentation," *IEEE Trans. Med. Imag.*, vol. 22, no. 9, pp. 1063–1075, Sep. 2003.

[21] K. S. Chuang, H. L. Tzeng, S. Chen, J. Wu, and T. J. Chen, "Fuzzy C-means clustering with spatial information for image segmentation," *Comput. Med. Imag. Graph.*, vol. 30, no. 1, pp. 9–15, Jan. 2006.

[22] Z. Ji, J. Liu, G. Cao, Q. Sun, and Q. Chen, "Robust spatially constrained fuzzy C-means algorithm for brain MR image segmentation," *Pattern Recognit.*, vol. 47, no. 7, pp. 2454–2466, Jul. 2014.

[23] F. F. Guo, X. X. Wang, and J. Shen, "Adaptive fuzzy C-means algorithm based on local noise detecting for image segmentation," *IET Image Process.*, vol. 10, no. 4, pp. 272–279, Mar. 2016.

[24] H. Verma, R. K. Agrawal, and A. Sharan, "An improved intuitionistic fuzzy C-means clustering algorithm incorporating local information for brain image segmentation," *Appl. Soft Comput.*, vol. 46, pp. 543–557, Sep. 2016.

[25] S. K. Adhikari, J. K. Sing, D. K. Basu, and M. Nisipuri, "Conditional spatial fuzzy C-means clustering algorithm for segmentation of MRI images," *Appl. Soft Comput.*, vol. 34, pp. 758–769, Sep. 2015.

[26] T. Lei, X. Jia, Y. Zhang, L. He, H. Meng, and A. K. Nandi, "Significantly fast and robust fuzzy C-means clustering algorithm based on morphological reconstruction and membership filtering," *IEEE Trans. Fuzzy Syst.*, vol. 26, no. 5, pp. 3027–3041, Oct. 2018.

[27] Y. Zhang, X. Bai, R. Fan, and Z. Wang, "Deviation-sparse fuzzy C-means with neighbor information constraint," *IEEE Trans. Fuzzy Syst.*, vol. 27, no. 1, pp. 185–199, Jan. 2019.

[28] C. Hwang and F. Rhee, "Uncertain fuzzy clustering: Interval type-2 fuzzy approach to C-means," *IEEE Trans. Fuzzy Syst.*, vol. 15, no. 1, pp. 107–120, Feb. 2007.

[29] O. Linda and M. Manic, "General type-2 fuzzy C-means algorithm for uncertain fuzzy clustering," *IEEE Trans. Fuzzy Syst.*, vol. 20, no. 5, pp. 883–896, Oct. 2012.

[30] R. Krishnapuram and J. M. Keller, "A possibilistic approach to clustering," *IEEE Trans. Fuzzy Syst.*, vol. 1, no. 2, pp. 98–110, May 1993.

[31] *BrainWeb: Simulated Brain Database*. Accessed: Aug. 2018. [Online]. Available: http://bic.mni.mcgill.ca/brainweb

[32] *Brain MR Image Database*. Accessed: Aug. 2018. [Online]. Available: http://www.cma.mgh.harvard.edu/ibsr

[33] F. Chung, H. Rhee, and C. Hwang, "A type-2 fuzzy C-means clustering algorithm," in *Proc. 20th NAFIPS Int. Conf. IFSA World Congr.*, 2001, pp. 1926–1929.

[34] J. M. Mendel, F. Liu, and D. Zhai, "á-plane representation for type-2 fuzzy sets: Theory and applications," *IEEE Trans. Fuzzy Syst.*, vol. 17, no. 5, pp. 1189–1207, Oct. 2009.

[35] K. Somasundaram and T. Kalaiselvi, "Automatic brain extraction methods for T1 Magnetic resonance images using region labeling and morphological operations," *Comput. Biol. Med.*, vol. 41, no. 8, pp. 716–725, Apr. 2011.

[36] K. Wu and M. S. Yang, "A cluster validity index for fuzzy clustering," *Pattern Recognit. Lett.*, vol. 26, pp. 1275–1291, Jul. 2005.

[37] P. Jaccard, "The distribution of the flora in the alpine zone," *New Phytol.*, vol. 11, no. 2, pp. 37–50, Feb. 2016.

[38] L. R. Dice, "Measures of the amount of ecologic association between species," *Ecology*, vol. 26, no. 3, pp. 297–302, Jul. 1945.

[39] J. Demsar, "Statistical comparisons of classifiers over multiple data sets," *J. Mach. Learn. Res.*, vol. 7, pp. 1–30, Jan. 2006.